Soliton States From Quadratic Electron-Phonon Interaction

Zhongjin Zhang, Anatoly Kuklov, Nikolay Prokof'ev, and Boris Svistunov^{1, 3}

¹Department of Physics, University of Massachusetts, Amherst, Massachusetts 01003, USA

²Department of Physics & Astronomy, CSI, and the Graduate Center of CUNY, New York 10314, USA

³ Wilczek Quantum Center, School of Physics and Astronomy and T. D. Lee Institute,

Shanghai Jiao Tong University, Shanghai 200240, China

We present the first numerically exact study of self-trapped, a.k.a. soliton, states of electrons that form in materials with strong quadratic coupling to the phonon coordinates. Previous studies failed to observe predictions based on the variational approach in continuum space because soliton states form only when system parameters are taken to the extreme limit. At the variational level, we establish that finite-radius solitons emerge through the weak first-order transition as the coupling strength is increased, and subsequently collapse to the single-site state through strong first-order transition. Both transitions transform into smooth crossovers between the light and heavy polaron states in the full quantum treatment. The most surprising effect not observed in any other polaron model is non-monotonic dependence of the soliton effective mass and the residue at strong coupling.

Introduction. For decades, studies of polarons—electrons renormalized by their coupling to lattice vibrations [1–3]—were focused on the linear density-displacement electron-phonon interaction (EPI):

$$H_{\rm int} = \sum_{\mathbf{kq}\sigma\alpha} V_{\mathbf{q}\alpha} c_{\mathbf{k}-\mathbf{q}\sigma}^{\dagger} c_{\mathbf{k}\sigma} \left[b_{\mathbf{q}\alpha}^{\dagger} + b_{-\mathbf{q}\alpha} \right], \qquad (1)$$

where α is the phonon branch index (we use standard notations for creation and annihilation operators for electrons $c_{\mathbf{k},\sigma}^{\dagger}, c_{\mathbf{k}\sigma}$ and phonons $b_{\mathbf{q}\alpha}^{\dagger}, b_{-\mathbf{q}\alpha}$ in momentum representation). The most popular models were the local Holstein [4, 5] and the non-local Frohlich [6, 7] models with $V_{\mathbf{q}\alpha} = \text{const}$ and $V_{\mathbf{q}\alpha} \propto 1/q$, respectively (for the recent review see Ref. [8]). More recently, researchers started exploring alternative interaction mechanisms based on the electron hopping amplitude dependence on atomic displacements [9–15] that bring an additional dependence of the vertex function in (1) on the incoming electron momentum, $V_{{f q}\alpha} \to V_{{f k},{f q}\alpha}$, but remain linear in the phonon coordinates. The interest in new models was motivated by their unusual properties and the possibility of having light but compact bi-polarons (bound states of two electrons) with high superconducting transition temperature [13, 16].

Much less explored and understood remained properties of polarons with quadratic EPI:

$$H_{\rm int} = g_2 \frac{\Omega}{4} \sum_{\mathbf{i}} n_{\mathbf{i}} [b_{\mathbf{i}}^{\dagger} + b_{\mathbf{i}}]^2. \tag{2}$$

Here Ω is the local oscillator frequency in the absence of coupling; it changes to $\tilde{\Omega} = \sqrt{1 + g_2 n_i} \Omega$ when the site is occupied. Note crucial dependence of the model's properties on the sign of g_2 and, in particular, the instability taking place at $g_2 < -1$.

An intriguing regime emerges when the two limits, $\Omega \to 0$ and $g_2 \to +\infty$, conspire to preserve finite $\tilde{\Omega}$. Indications of the importance of this regime were found in several materials: doped manganites [17], halide perovskites [18], and quantum paraelectrics [19, 20]. The

soft vibration modes in these materials are transverse optical phonons for which the linear EPI is suppressed in the long-wave limit [21–25]; similar physics takes place in optically pumped systems [26, 27]. Early suggestions that bi-phonon exchange could be an important pairing mechanism at low doping [21] were recently revisited and used to explain superconductivity in SrTiO₃ [28– 30]. However, dealing with non-linear couplings theoretically beyond perturbation theory has been challenging. The original work [22–25] was based on the variational solution for large-radius soliton states in continuum. The momentum average approximation [31] was used to study a combination of linear and nonlinear EPI in Refs. [32, 33]. More recently, nonlinear EPI effects were investigated in Refs. [34–36] using the determinant Monte Carlo method [37] for finite 2D systems at high electron density and finite temperature. Finally, the interplay between the linear and quadratic EPI in continuum was studied in Ref. [38] by the variational Feynman's path-integral method [39].

The situation has changed with the development of the numerically exact x-representation Monte Carlo (XMC) technique for polaron problems with arbitrary nonlinear density-displacement and arbitrary sign-preserving hopping-displacement interactions [40]. It was used to obtain the first precise results for quadratic EPI (2) at strong coupling [41], but the study failed to observe soliton states predicted by Ref. [22, 23] (in what follows we will call them "kuklons") despite considering relatively small adiabatic parameter $\gamma = \Omega/W = 1/48$, where W = 12t is the bandwidth of the 3D tight-binding model on the cubic lattice with the nearest-neighbor hopping amplitude t. Thus, no progress on the soliton problem was made for more than three decades, and it remains unknown how and under what conditions these states form and what their basic properties are.

In this Letter, we first expand the variational analysis of the adiabatic limit to reveal how kuklons form and then collapse in first-order phase transitions. Next, we

present results of the numerically exact studies of kuklons by the XMC method in the parameter regime that is orders of magnitude beyond the limitations of all other known schemes: $\gamma=1/600$ and $\gamma=1/2400$ with g_2 as large as 10^8 . In the full quantum solution, the first-order transitions are transformed into smooth crossovers with the most unusual (not observed in any other polaron problem) non-monotonic dependence of the effective mass and Z-factor on g_2 at strong coupling.

Hamiltonian, effective adiabatic model, and methods. The full system's Hamiltonian on the simple cubic lattice reads

$$H = 6t - t \sum_{\langle ij \rangle} c_i^{\dagger} c_j + \Omega \sum_i b_i^{\dagger} b_i + H_{\text{int}}.$$
 (3)

[The phonon energy is counted from the ground state of the unperturbed harmonic oscillator.] In the adiabatic, $\gamma \to 0$, limit one takes advantage of the fact that electrons are much faster than phonons and the contribution of the latter to energy depends solely on the average electron density distribution [1, 2, 22, 23]. For model (3), these standard considerations lead to the following energy functional to be minimized:

$$E = 6t - t \sum_{\langle ij \rangle} \psi_i^* \psi_j + \frac{\Omega}{2} \sum_i \left(\sqrt{1 + g_2 |\psi_i|^2} - 1 \right).$$
 (4)

Here ψ is the normalized electron wave function (real for the ground state), and the last term is the sum of ground-state energies for each oscillator. Given that oscillator frequencies increase with g_2 , the adiabatic condition for the polaron of radius R is satisfied if $\sqrt{R^{-3}g_2}\Omega \ll t/R^2$ or $g_2 \ll (t/\Omega)^2/R$ (the lattice constant a=1 serves as the unit of length). For large-radius kuklon, we also consider a continuous counterpart of Eq. (4) with m=1/2t:

$$E = \int d^3r \left[\frac{1}{2m} |\nabla \psi|^2 + \frac{\Omega}{2} \left(\sqrt{1 + g_2 |\psi|^2} - 1 \right) \right]. \quad (5)$$

Minimization of Eq. (4) is achieved by the gradient decent method when at each stage the wave function is first transformed according to $\tilde{\psi} = \psi - \epsilon \nabla_{\psi} H$ and then normalized to unity. This step is rejected and the value of ϵ is decreased by a factor of two if $E[\tilde{\psi}] > E[\psi]$; otherwise it is accepted. For optimal solutions we record their energies and root mean square radii, $R = \sqrt{\langle r^2 \rangle}$, where $\langle r^2 \rangle = \sum_i r_i^2 \psi_i^2$. We ensure that all finite-size effects are exponentially small for the polaron solutions presented in this paper (realistically, one can work with about 300^3 sites after utilizing system symmetries).

Numerically exact solutions of (3) are obtained using recently developed XMC method based on the lattice path integral for the electron and coordinate representation for harmonic oscillators (see Refs. [40, 41] for complete description). Key polaron properties such as

dispersion relation, E_p , ground-state energy, $E=E_{p=0}$, effective mass, $1/m^*=d^2E_{p=0}/dp^2$, and the quasiparticle residue, $Z=Z_{p=0}$, are obtained from simulations of the polaron Green's function, $G_p(\tau)$, and its asymptotic behavior, $G_p(\tau) \to Z_p \mathrm{e}^{-E_p \tau}$, in the $\tau \to \infty$ limit.

Variational analysis. The formation of kuklons is driven by competition between the hopping term favoring delocalized states and EPI repulsion preferring localized states due to sub-linear dependence of the interaction energy on density at strong coupling [last terms in (4) and (5)]. Since delocalized states correspond to $\psi_i \to 0$, their variational energy readily follows from Eq. (4) in this limit: $E_0 = g_2\Omega/4$.

Localized continuous solutions at strong coupling were obtained in Ref. [22, 23]. If the last term in (5) is approximated as $\Omega\sqrt{g_2}|\psi|/2$, then energy minimization reduces to the solution of the radial eigenvalue equation, $-d^2\psi/dr^2 + m\Omega\sqrt{g_2}/2 - \lambda\psi = 0$, with the solution

$$\psi(r) = \sqrt{\frac{3}{10\pi R_A^3}} \left[1 - \frac{R_A \sin(x_0 r / R_A)}{r \sin(x_0)} \right], \quad (6)$$

for $r < R_A$ and $\psi(r) = 0$ for $r \ge R_A$, where $x_0 \approx 4.49$ is the lowest positive root of $\tan x = x$ and R_A is the cut-off radius, $R_A = [6x_0^4/(5\pi g_2\Omega^2 m^2)]^{1/7}$. The root mean-square radius of this solution is given by $R = (11/25 - 49/10x_0^2)^{1/2}R_A \approx 0.444R_A$ and its energy

$$E_A = \frac{7}{10} \left(\frac{5\pi x_0^3}{6} \right)^{2/7} \frac{\left(g_2 \Omega^2 \right)^{2/7}}{m^{3/7}} \approx 3.34 \frac{\left(g_2 \Omega^2 \right)^{2/7}}{m^{3/7}}. \quad (7)$$

falls below $g_2\Omega/4$ for $g_2 > 37.7(m\Omega)^{-3/5}$.

Thus, on the one hand, kuklons form at strong coupling $g_2\gg 1$. On the other hand, this coupling needs to be small enough to ensure adiabaticity of the state and its large radius because at $g_2>(t/\Omega)^2$ both conditions are violated. At $g_2\gg (t/\Omega)^2$ the polaron state is well described by the so-called atomic limit (AL) when the electron changes frequency only of the harmonic oscillator at the occupied site, see Ref. [41]. Physically, this is a completely different state characterized by $R\approx 0$ and $E_{\rm atom}\approx \frac{\Omega}{2}(\sqrt{1+g_2}-1)$.

In a more precise treatment, the last term in (5) is dealt with "as is" and the cutoff at R_A gets replaced with gradual exponential decay of the wavefunction with distance; this feature is important for correct description of the transition between the localized and delocalized states. The corresponding numerical analysis is presented below. In the absence of hard cutoff, we have to resort to the root mean square radii for defining the polaron size.

To study properties of kuklons away from the asymptotic adiabatic limit $(\gamma \to 0, R \to \infty)$ —how they first form and then transition to the AL state, we resort to the exact minimization of the lattice functional (4) by gradient decent. Using t=1 as the energy unit, we first consider the case of extremely small phonon frequency

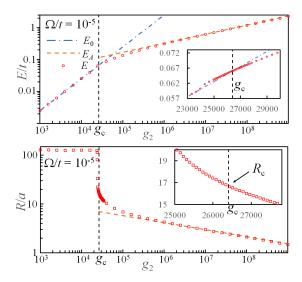


FIG. 1. (color online) Energy (upper panel, red circles) and radius (lower panel, red squares) of lattice variational states as functions of g_2 for $\Omega/t = 10^{-5}$. Dashed (orange) lines are the asymptotic continuous solutions, see Eq. (7) and the text above. Dash-dotted (blue) line is energy of the delocalized state. Insets: Energy and radius vs. g_2 near the critical point.

 $\Omega/t = 10^{-5}$, see Fig. 1. For $g_2 \gg g_c$ ($g_c = 26406$), both E and R are accurately described by the asymptotic continuous solutions. However, this is no longer the case on approach to g_c , because exact variational solutions remain stable at significantly smaller (by a factor of two) values of g_2 as their volume undergoes a rapid expansion (by nearly an order of magnitude). This is a clear indication that the hard-cutoff approximation is not reliable near the critical point.

Close examination of the $|g_2 - g_c|/g_c \ll 1$ region, see insets in Fig. 1, reveals that within the variational treatment, kuklons with finite radius R_c emerge through a weak first-order transition. Indeed, for g_2 slightly smaller than g_c , we detect metastable localized solutions (obtained by starting from an initial wave function with a small radius), which subsequently disappear at $g_2 < 0.92g_c$. The phase transition point can be located very accurately from the intersection of the E and E_0 curves.

In continuum, the energy functional is invariant under the scaling transformation, $r \to br$, $g_2 \to b^3 g_2$, $\Omega \to b^{-3}\Omega$, and $m \to b^{-2}m$. Moreover, if m and Ω are changed while keeping the adiabatic parameter $m\Omega$ constant, the functional is simply multiplied by a factor $\tilde{\Omega}/\Omega$. Thus, upon proper scaling, we are left with only one free parameter: g_2 . These considerations imply that the critical coupling and radius scale as $g_c \propto (m\Omega)^{-3/5}$ and $R_c \propto (m\Omega)^{-1/5}$. On a lattice, this scaling is expected to fail when $R_c \sim a$. Data in Fig. 3 demonstrate

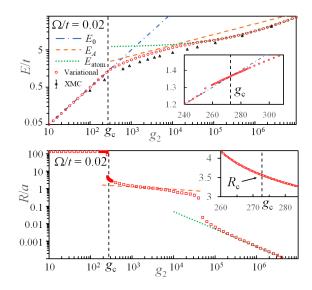


FIG. 2. (color online) Upper panel: Energies of variational states (red cicles) in comparison with XMC results (black triangles) for $\Omega=0.02$. Lower panel: variational state radii (red squares). Dashed (orange) lines are predictions of the asymptotic continuous solutions. Dash-dotted (blue) line is the energy of the delocalized variational state E_0 . Dotted (green) line is the atomic limit energy $E_{\rm atom}$. Inset: Variational E vs. g_2 near the critical point.

the accuracy of this prediction for large critical sizes.

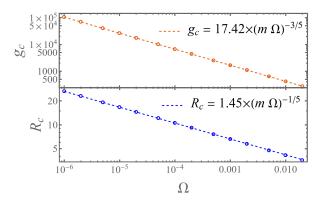


FIG. 3. Critical coupling and radius of kuklons in continuum as a function of Ω . Both show clear power-law dependence (dashed lines) with expected exponents.

Quantum solution. For a less extreme but still small adiabatic ratio $\gamma=1/600$ we are posed to compare variational and full quantum solutions, see Fig. 2. As expected, the first-order transition at $g_c=272.7$ predicted by (4) is replaced with smooth quantum crossover. Despite very small value of γ the exact energy is still significantly different from its variational counterpart across the crossover region. This surprising outcome finds its explanation in relatively small kuklon sizes predicted by

(4): about four lattice spacings at g_c and quickly shrinking to $R \sim a$ in a broad parameter range. Quantum effects are expected to be pronounced at the lattice scale not to mention that for $R \sim a$ the adiabatic condition also becomes questionable. Nevertheless, it is clear that at $g_2 \sim 10^3$ the polaron state undergoes a radical transformation from perturbative plane-wave state with slightly renormalized effective mass and $Z \approx 1$ to a state with m^*/m much larger and Z-factor much smaller than what is expected in the AL, see upper panels in Fig. 4. These results imply that the electron is "dressed" by oscillator excitations distributed over multiple sites, i.e. it forms a kuklon.

We observe that parameters required for formation of large-radius kuklons are extreme and well beyond the limits of applicability of any other unbiased method. For XMC, simulations of $\gamma < 0.001$ are also very challenging in the regime of large effective masses, $m^*/m \gtrsim 1000$, and exponentially small Z-factors. This explains why previous numerical studies failed to see them.

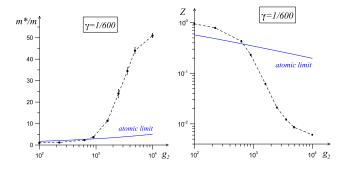


FIG. 4. (color online) Effective mass and Z-factor for $\Omega/t = 0.02$ as functions of g_2 from the XMC method. Solid lines are results expected in the atomic limit

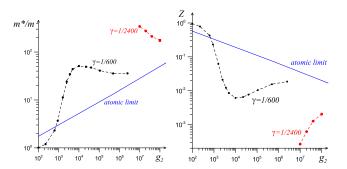


FIG. 5. (color online) Effective masses and Z-factors for $\Omega/t = 0.02$ and $\Omega/t = 0.005$ as functions of g_2 over a much broader range that in Fig. 4. Solid lines are results expected in the atomic limit.

Collapse to the atomic limit. Lighter polarons at stronger coupling. Once kuklons form, their radius grad-

ually decreases with coupling and at $g_2 \sim (t/\Omega)^2$ both lattice effects and non-adiabatic corrections come into play. Naive expectations are that AL is nothing but the end of the smooth monotonic evolution of the kuklon state. This turns out to be incorrect and in a rather dramatic fashion. Figure 2 shows that the lattice functional features a second transition at large g_2 , this time between the kuklon and AL states. It can be understood analytically by restricting analysis to just two wave function components near the transition point: $\psi_0 \simeq 1$ at the center and $\psi_1 \ll 1$ at the six nearest neighbour sites (other components are proportional to higher powers of ψ_1). By assuming that $\psi_1^2 g_2 \gg 1$ and using the normalization condition, $\psi_0^2 = 1 - 6\psi_1^2$, we arrive at the energy dependence on ψ_1

$$E/t = 6 \left[6\psi_1^3 - \chi \psi_1^2 + 2(\chi - 1)\psi_1 \right] + \text{const}$$
 (8)

that features a first-order transition when $\chi = \sqrt{g_2}\Omega/(4t) = \chi_c$, with $\chi_c \approx 1.022$. At this level of description, the transition is from small but non-zero ψ_1 at $\chi < \chi_c$ to $\psi_1 = 0$ at $\chi > \chi_c$. In terms of the coupling constant, the transition takes place at $g_2 > (4t/\Omega)^2 = 9/\gamma^2$. [The above consideration is valid only in the $\gamma \to 0$ limit; more precise treatment with terms $\propto \chi/(g_2\psi_1)$ included shows that the discontinuous transition to the AL takes place only for $\gamma < 0.0015$.]

While there is no reason to trust variational results for compact states, they do point to the possibility of having a much faster crossover to the AL than what is expected in terms of slow power-low evolution $R \propto g_2^{-1/7}$. Given an order of magnitude difference between the effective masses and Z-factors of the kuklon and AL states, see Fig. 4, monotonic power-law transformation of one state into another would require enormous values of g_2 . But if this transformation takes the form of a more rapid crossover then m^* and Z must exhibit non-monotonic dependence on g_2 at strong coupling. Such highly counterintuitive behavior was never reported for any polaron problem. By extending XMC simuations to much larger values of g_2 for $\gamma = 1/600$ and performing additional simulations for $\gamma = 1/2400$ at strong coupling we do observe the non-monotonic dependence of m^* and Z (more pronounced for smaller γ), see Fig. 4, i.e. kuklons are getting lighter as they approach AL.

Conclusions. We performed detailed studies of soliton (kuklon) states in the model with strong quadratic electron-phonon interaction by (i) extending previous variational analysis to lattice systems, (ii) revealing two first-order transitions and their properties, which explain how kuklons form and subsequently collapse to the single-site states at the variational level, and (iii) solving the problem numerically exactly by the X-representation Monte Carlo technique. In exact solutions, transitions are replaced by smooth crossovers with rapid increase of the effective mass and decrease of the quasiparticle

residue at strong coupling. An opposite trend is discovered when the soliton size is of the order of the lattice spacing.

Previous numerical work failed to see kuklons because they form when system parameters take values way beyond the limitations of all other unbiased methods. Future work should explore properties of bi-polaron states in the same model; bound states are expected to form in the same parameter regime where kuklons form and for the same reason—sublinear dependence of the interaction energy on electron density. Figure 4 suggests that it is possible to have light and compact bi-polarons, which is a prerequisite for high superconducting temperature at finite density [13, 16].

We acknowledge support from the National Science Foundation under Grants No. DMR-2032136 and No. DMR-2032077.

- [1] L. Landau, Phys. Z. Sowjetunion 3, 664 (1933).
- [2] S. Pekar, Zh. Eksp. Teor. Fiz. 16, 335 (1946).
- [3] L. Landau and S. Pekar, Zh. Eksp. Teor. Fiz. 18, 419 (1948).
- [4] T. Holstein, Ann. Phys. 8, 325 (1959).
- [5] T. Holstein, Ann. Phys. 281, 725 (2000).
- [6] H. Fröhlich, H. Pelzer, and S. Zienau, Philos. Mag. 41, 221 (1950).
- [7] H. Fröhlich, Adv. Phys. 3, 325 (1954).
- [8] C. Franchini, M. Reticcioli, M. Setvin, and U. Diebold, Nature Reviews Materials 6, 560 (2021).
- [9] D. Marchand, G. De Filippis, V. Cataudella, M. Berciu, N. Nagaosa, N. Prokof'ev, A. Mishchenko, and P. Stamp, Phys. Rev. Lett. 105, 266605 (2010).
- [10] J. Sous, M. Chakraborty, R. Krems, and M. Berciu, Phys. Rev. Lett. 121, 247001 (2018).
- [11] B. Xing, W.-T. Chiu, D. Poletti, R. Scalettar, and G. Batrouni, Phys. Rev. Lett. 126, 017601 (2021).
- [12] C. Zhang, N. Prokof'ev, and B. Svistunov, Phys. Rev. B 104, 035143 (2021).
- [13] C. Zhang, J. Sous, D. Reichman, M. Berciu, A. Millis, N. Prokof'ev, and B. Svistunov, Phys. Rev. X 13, 011010 (2023).
- [14] M. Carbone, A. Millis, D. Reichman, and J. Sous, Phys. Rev. B 104, L140307 (2021).
- [15] J. Sous, C. Zhang, M. Berciu, D. Reichman, B. Svistunov, N. Prokof'ev, and A. Millis, arXiv:2210.14236 (2022).
- [16] C. Zhang, B. Capogrosso-Sansone, M. Boninsegni,

- N. Prokof'ev, and B. Svistunov, Phys. Rev. Lett. **130**, 236001 (2023).
- [17] V. Esposito, M. Fechner, R. Mankowsky, H. Lemke, M. Chollet, J. M. Glownia, M. Nakamura, M. Kawasaki, Y. Tokura, U. Staub, P. Beaud, and M. Först, Phys. Rev. Lett. 118, 247601 (2017).
- [18] M. Schilcher, P. Robinson, D. Abramovitch, L. Tan, A. Rappe, D. Reichman, , and D. Egger, ACS Energy Lett. 6, 2162 (2021).
- [19] A. Kumar, V. I. Yudson, and D. L. Maslov, Phys. Rev. Lett. 126, 076601 (2021).
- [20] K. G. Nazaryan and M. V. Feigel'man, Phys. Rev. B 104, 115201 (2021).
- [21] K. L. Ngai, Phys. Rev. Lett. 32, 215 (1974).
- [22] A. Kuklov, Physics Letters A 139, 270 (1989)
- [23] A. B. Kuklov, Superconductivity 3, S355 (1990), ISSN 0235-8964 [translation from Russian, Sverkhprovodimost (KIAE), 3 (10), 2277 (1990)].
- [24] A. Gogolin and A. Ioselevich, JETP letters 53, 479 (1991).
- [25] A. Gogolin and A. Ioselevich, JETP letters 54, 285 (1991).
- [26] D. Kennes, E. Wilner, D. Reichman, and A. Millis, Nat. Phys. 13, 479 (2017).
- [27] J. Sous, B. Kloss, D. Kennes, D. Reichman, and A. Millis, Nat. Comm. 12, 5803 (2021).
- [28] D. van der Marel, F. Barantani, and C. W. Rischau, Phys. Rev. Res. 1, 013003 (2019).
- [29] P. Volkov, P. Chandra, and P. Coleman, Nat. Comm. 13, 4599 (2022).
- [30] D. E. Kiselov and M. V. Feigel'man, Phys. Rev. B 104, L220506 (2021).
- [31] M. Berciu, Phys. Rev. Lett. 97, 036402 (2006).
- [32] C. Adolphs and M. Berciu, Europhys. Lett. 102, 47003 (2013).
- [33] C. P. J. Adolphs and M. Berciu, Phys. Rev. B 89, 035122 (2014).
- [34] S. Li and S. Johnston, Europhys. Lett. 109, 27007 (2015).
- [35] S. Li, E. A. Nowadnick, and S. Johnston, Phys. Rev. B **92**, 064301 (2015).
- [36] P. Dee, J. Coulter, K. Kleiner, and S. Johnston, Commun. Phys. 3, 145 (2020).
- [37] S. Johnston, E. A. Nowadnick, Y. F. Kung, B. Moritz, R. T. Scalettar, and T. P. Devereaux, Phys. Rev. B 87, 235133 (2013).
- [38] M. Houtput and J. Tempere, Phys. Rev. B 103, 184306 (2021).
- [39] R. P. Feynman, Phys. Rev. 97, 660 (1955).
- [40] N. Prokof'ev and B. Svistunov, Phys. Rev. B 106, L041117 (2022).
- [41] S. Ragni, T. Hahn, Z. Zhang, N. Prokof'ev, A. Kuklov, S. Klimin, M. Houtput, B. Svistunov, J. Tempere, N. Nagaosa, C. Franchini, and A. Mishchenko, Phys. Rev. B 107, L121109 (2023).